Homography-Based Visual Servo Regulation of Mobile Robots

Yongchun Fang, *Member, IEEE*, Warren E. Dixon, *Member, IEEE*, Darren M. Dawson, *Senior Member, IEEE*, and Prakash Chawda, *Student Member, IEEE*

***Abstract*—A monocular camera-based vision system attached to a mobile robot (i.e., the camera-in-hand configuration) is considered in this paper. By comparing corresponding target points of an object from two different camera images, geometric relationships are exploited to derive a transformation that relates the actual position and orientation of the mobile robot to a reference position and orientation. This transformation is used to synthesize a rotation and translation error system from the current position and orientation to the fixed reference position and orientation. Lyapunov-based techniques are used to construct an adaptive estimate to compensate for a constant, unmeasurable depth parameter, and to prove asymptotic regulation of the mobile robot. The contribution of this paper is that Lyapunov techniques are exploited to craft an adaptive controller that enables mobile robot position and orientation regulation despite the lack of an object model and the lack of depth information. Experimental results are provided to illustrate the performance of the controller.**

***Index Terms*—Adaptive control, homography, Lyapunov techniques, visual servo.**

I. Introduction

BASED on the success of image extraction/interpretation technology and advances in control theory, research has focused on the use of monocular camera-based vision systems for navigating a mobile robot [18], [33], [34], [36]. A significant issue with monocular camera-based vision systems is the lack of depth information. From a review of literature, various approaches have been developed to address the lack of depth information inherent in monocular vision systems. For example, using consecutive image frames and an object database, Kim *et al.* [20] recently proposed a mobile robot tracking controller based on a monocular visual feedback strategy. To achieve their result, they linearized the system equations using a Taylor series approximation, and then applied extended Kalman filtering (EKF) techniques to compensate for the lack of depth information [20]. Also using EKF techniques on the linearized kinematic model, Das *et al.* [10] used feedback from a monocular omnidirectional camera system (similar to [1]) to enable wall following, follow-the-leader, and position regulation tasks. Jung *et al.* [19] exploited an object model and Kalman filtering techniques to estimate the unknown depth information and achieve a tracking result for a monocular mobile robot system. Unfortunately, a clear drawback of using EKF techniques to estimate depth information is the requirement for linearization. Song and Huang [30] use spatiotemporal apparent velocities obtained from an optical flow of successive images to estimate the depth information for a monocular "guide robot." An optical flow estimation technique was also developed in [22]. However, typical drawbacks of optical flow techniques include the need for temporal smoothing and excessive image processing to determine the image flow; resulting in an intensive computational burden for real-time robotics control.

Dixon *et al.* [12] used feedback from an uncalibrated, fixed (ceiling-mounted) camera to develop an adaptive tracking controller for a mobile robot that compensated for the parametric uncertainty in the camera and the mobile robot dynamics. Dixon *et al.* exploit Lyapunov-based adaptive techniques to compensate for the unknown depth information [12]. However, to employ these techniques, they require the depth from the camera to the mobile robot plane of motion to remain constant (i.e., the camera plane and the mobile robot plane must be parallel). This assumption reduces the nonlinear pinhole camera model to a decoupled linear transformation; however, it also restricts the applicability of the controller. Recently, Chen *et al.* [6] developed a mobile robot visual servo tracking controller when the camera is onboard. An advantage of the result in [6] is that the mobile robot is not constrained to a planar application and an adaptive estimate is provided to compensate for unknown time-varying depth information. However, the development in [6] and [12] cannot be applied to solve the mobile robot regulation problem due to restrictions on the mobile robot reference velocity (i.e., the reference linear velocity cannot converge to zero). Wang *et al.* [35] also exploit a Lyapunov-based adaptive technique to compensate for a constant unknown depth parameter for a monocular mobile robot tracking problem. While the approach in [35] may be well suited for tracking applications, the stability analysis requires the same restrictions on the reference trajectory of the mobile robot as in [12], and hence, cannot be applied to solve the regulation problem. Hager *et al.* [17] used a monocular vision system mounted on a pan-tilt-unit to generate image-Jacobian and geometry-based controllers by using

Manuscript received November 15, 2004; revised February 16, 2005. This work was supported in part by the Air Force Office of Scientific Research under Contract F49620-03-1-0381 at the University of Florida, in part by the Department of Commerce, in part by the U.S. Army Research Office (ARO) under an ARO Automotive Center Grant, in part by the Department of Energy, in part by the Honda Corporation, and in part by the Defense Advanced Research Projects Agency (DARPA) under DARPA Contract with Clemson University. This paper was recommended by Associate Editor T. H. Lee.

Y. Fang is with the Institute of Robotics and Automatic Information System, Nankai University, Tianjin 300071, China (e-mail: yfang@robot.nankai.edu.cn).

W. E. Dixon is with the Department of Mechanical and Aerospace Engineering, University of Florida, Gainesville, FL 32611 USA (e-mail: wdixon@ufl.edu).

D. M. Dawson and P. Chawda are with the Department of Electrical and Computer Engineering, Clemson University, Clemson, SC 29634-0915 USA (e-mail: ddawson, pchawda@ces.clemson.edu).

Digital Object Identifier 10.1109/TSMCB.2005.850155

different snapshots of the target and an epipolar constraint. As stated in [3], a drawback of the method developed in [17] is that the system equations became numerically ill-conditioned for large pan angles. Given this shortcoming, Burschka and Hager [3] used a spherical image projection of a monocular vision system to overcome the limitations of [17]. Specifically, offline teaching and replay phases are used in [3] as a means to develop a static estimation of a constant depth-related parameter. A drawback of this offline learning technique is that the process generates an estimate for a single mobile robot motion, and to achieve better results, every system motion would need to be taught requiring a least squares problem to be solved to generate the estimate.

Recently, a monocular two-and-one-half-dimensional (2.5-D) visual servo control methodology was developed for unconstrained systems (e.g., robot manipulators) in a series of papers by Malis and Chaumette (e.g., [4], [5], [25]–[27]). Specifically, the 2.5-D visual servo control method exploits a combination of reconstructed three-dimensional (3-D) task-space information and two-dimensional (2-D) image-space information. The 3-D information is reconstructed by decoupling the interaction between translation and rotation components of a Euclidean homography. As stated in [27], some of the advantages of this methodology include: 1) an accurate 3-D model of the environment (or target image) is not required; 2) the control exploits pixel information which increases the potential to force the target to remain in the camera field-of-view; 3) local minima can be avoided; and 4) singularities only exist in the image-Jacobian in degenerate cases. Based on the observation that interaction between the translation and rotation of images can result in slower transient performance due to inefficient camera motions, Deguchi proposed two algorithms in [11] for a robot manipulator application that decouple the rotation and translation components using a homography and an epipolar condition. More recently, Corke and Hutchinson [9] also developed a method for decoupling the rotation and translation components from the remaining degrees of freedom using a new hybrid image-based visual servoing scheme. Motivated by the desire to compensate for the aforementioned depth information, [8] developed an adaptive kinematic controller for a robot manipulator application to ensure uniformly ultimately bounded (UUB) set-point regulation of the image point errors while compensating for the unknown depth information, provided conditions on the translational velocity and the bounds on uncertain depth parameters are satisfied. Unfortunately, these approaches typically assume that a constant best guess estimate of a depth-related parameter can be used in lieu of the actual parameter, but the effects of the parameter mismatch are not included in the stability analysis. Recently, Chen *et al.* [7] developed a homography-based visual servo controller for robot manipulator systems that adaptively compensates for the unknown time-varying depth parameter for a monocular camera system mounted in the camera-in-hand and fixed-camera configurations.

In this paper, asymptotic regulation of the position/orientation of a mobile robot is achieved by exploiting homography-based visual servo control strategies inspired by the work given in [4], [5], [26], and [27]. By comparing the features of an object in the reference image to features of the object in the current image,

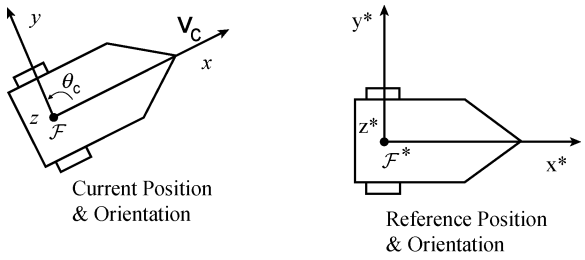

Fig. 1. Mobile robot coordinate systems.

image-based geometric relationships are exploited to construct a homography matrix despite the fact that a geometric model of the object is not known. By decomposing the homography into separate translation and rotation components, measurable signals for the orientation and the scaled Euclidean position can be obtained. Full Euclidean reconstruction is not possible due to the lack of an object model and the lack of depth information from the onboard camera to the target; hence, the resulting translation error system is unmeasurable. To accommodate for the lack of depth information, the unknown time-varying depth information is related to a constant depth-related parameter. The closed-loop error systems are then constructed using Lyapunov-based methods including the development of an adaptive estimate for the constant depth-related parameter. The contribution of this paper is that Lyapunov techniques are exploited to craft an adaptive controller that enables mobile robot position and orientation regulation despite the lack of an object model and the lack of depth information. Due to assumptions on the reference trajectory resulting from the nonholonomic constraint, the aforementioned visual servo tracking control results cannot be applied to solve the regulation problem considered in the current result. For example, in comparison with our previous efforts in [6], the current controller is completely redesigned to overcome restrictions inherent to the controller in [6] to solve the regulation result. See [14], [21], and [24] for a more technically detailed description of the issues and differences associated with developing tracking and regulation controllers for nonholonomic systems. The result in this paper is achieved with a monocular vision system, and the adaptive control design approach incorporates the full nonlinear kinematic equations of motion. Experimental results are provided to illustrate the performance of the developed controller. A practical issue with the presented research is that the feature points may leave the camera's field of view during task execution. To address this problem, future efforts will target regulating the mobile robot while ensuring the feature points remain visible.

II. Problem Formulation

The objective of this paper is to regulate the position/orientation of a mobile robot based on image-feedback of a fixed target. As illustrated in Fig. 1, the origin of the orthogonal coordinate system $\mathcal{F}$ attached to the camera is coincident with the center of mass of the mobile robot. As also illustrated in Fig. 1, the xy axis of $\mathcal{F}$ defines the mobile robot plane of motion where the x axis of $\mathcal{F}$ is aligned with the front of the mobile robot, and the y axis is parallel to the wheel axis. The z axis of $\mathcal{F}$ is perpendicular to the mobile robot plane of motion and is located at the

center of the wheel axis. The linear velocity of the mobile robot along the x axis is denoted by $v_c(t)$, and the angular velocity $\omega_c(t)$ is about the x axis. In addition to $\mathcal{F}$, another fixed orthogonal coordinate system, denoted by $\mathcal{F}^*$, is defined to represent the desired fixed position and orientation of the camera relative to a target. Hence, the goal is to develop a controller that will regulate the position and orientation of $\mathcal{F}$ to $\mathcal{F}^*$.

III. Camera Model

In this paper, the target is assumed to be distinguished by three points O_i, $i = 1, 2, 3$ that compose a plane, denoted by π. The Euclidean position of point O_i expressed in the coordinate frames $\mathcal{F}$ and $\mathcal{F}^*$ is denoted by $\bar{m}_i(t)$, $\bar{m}_i^* \in \mathbb{R}^3$, respectively, and is defined as follows (see Fig. 2):

$$\bar{m}_i(t) \triangleq [x_i(t) \quad y_i(t) \quad z_i(t)]^T \qquad \bar{m}_i^* \triangleq [x_i^* \quad y_i^* \quad z_i^*]^T. \tag{1}$$

Since the 3-D Euclidean position of the point O_i is observed from the 2-D image-space of the camera, normalized position vectors are defined as follows:

$$\begin{aligned} m_i(t) &\triangleq [1 \quad m_{iy}(t) \quad m_{iz}(t)]^T = \frac{\bar{m}_i(t)}{x_i(t)} \\ &\triangleq \begin{bmatrix} 1 & \dfrac{y_i(t)}{x_i(t)} & \dfrac{z_i(t)}{x_i(t)} \end{bmatrix}^T \\ m_i^* &\triangleq [1 \quad m_{iy}^* \quad m_{iz}^*]^T = \frac{\bar{m}_i^*}{x_i^*} \\ &\triangleq \begin{bmatrix} 1 & \dfrac{y_i^*}{x_i^*} & \dfrac{z_i^*}{x_i^*} \end{bmatrix}^T \end{aligned} \tag{2}$$

where the standard assumption is made that $x_i(t)$ and x_i^* are positive [27] (i.e., the target is always in front of the camera). In addition to the normalized Euclidean position, each point has an image-space representation, denoted by $p_i(t)$, $p_i^* \in \mathbb{R}^3$

$$p_i(t) \triangleq [1 \quad u_i(t) \quad v_i(t)]^T \qquad p_i^* \triangleq [1 \quad u_i^* \quad v_i^*]^T \tag{3}$$

where $u_i(t)$, $v_i(t) \in \mathbb{R}$ denote the pixel coordinates of the point O_i. The image-space coordinates given in (3) are related to the normalized coordinates given in (2) by the following invertible transformation (i.e., the pinhole camera model):

$$m_i = A^{-1} p_i \quad m_i^* = A^{-1} p_i^* \tag{4}$$

where $A \in \mathbb{R}^{3\times 3}$ denotes a constant, invertible matrix composed of the intrinsic camera calibration parameters [27]. Since the camera is assumed to be calibrated (i.e., the matrix A is assumed to be known), $m_i(t)$ and m_i^* can be calculated using (4) from the known camera pixel-space vectors $p_i(t)$ and p_i^*.

The main idea behind the current visual servoing strategy is to extract 2-D information from the environment using the camera image and then determine 3-D information through a Euclidean reconstruction. The Euclidean reconstruction is performed by exploiting the geometry between the features of the target (image points) in the camera's current image to the desired image. Based on the geometric relationships, a homography matrix can be calculated to relate the projected 3-D position to the image-space position of the target [16], [27], [37]. For example, the geometric relationships between $\mathcal{F}$ and $\mathcal{F}^*$ can be determined from Fig. 2. In Fig. 2, $\theta(t) \in \mathbb{R}$ is the angle between the axes x^* and x, the unit vectors $n(t)$, $n^* \in \mathbb{R}^3$ are normal to the plane π expressed in $\mathcal{F}$ and $\mathcal{F}^*$, respectively, and $d(t)$, $d^* \in \mathbb{R}$ are the unknown, positive distances from the origin of $\mathcal{F}$ and $\mathcal{F}^*$ to the plane π along n and n^*, respectively. Based on Fig. 2, the following relationship can be determined:

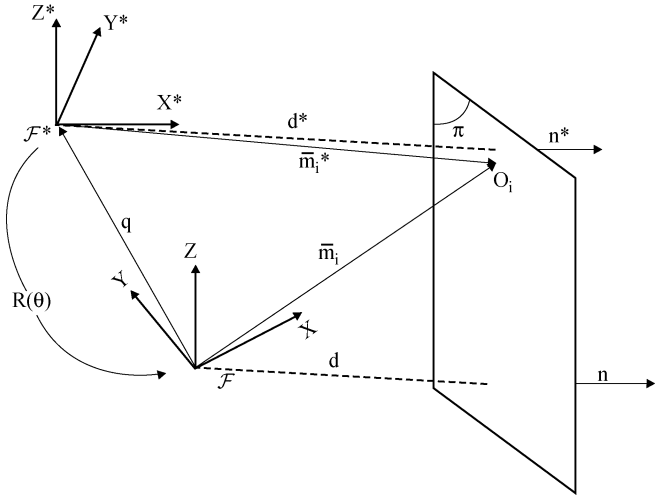

Fig. 2. Geometric relationship of the mobile robot system.

$$\bar{m}_i = R\bar{m}_i^* + q. \tag{5}$$

In (5), $R(t) \in SO(3)$ denotes the following rotation matrix from $\mathcal{F}^*$ to $\mathcal{F}$:

$$R \triangleq \begin{bmatrix} \cos(\theta) & -\sin(\theta) & 0 \\ \sin(\theta) & \cos(\theta) & 0 \\ 0 & 0 & 1 \end{bmatrix} \tag{6}$$

and $q(t) \in \mathbb{R}^3$ is the translation vector from $\mathcal{F}$ to $\mathcal{F}^*$ given by

$$q(t) \triangleq [q_x(t) \quad q_y(t) \quad 0]^T. \tag{7}$$

Since d^* is the projection of $\bar{m}_i^*$ along n^*, the following relationship can be determined:

$$d^* = (n^*)^T \bar{m}_i^*. \tag{8}$$

Using (8), the expression given in (5) can be rewritten as

$$\bar{m}_i = H\bar{m}_i^* \tag{9}$$

where the Euclidean homography $H(t) \in \mathbb{R}^{3\times 3}$ is defined as follows:

$$H \triangleq R + \frac{q}{d^*}(n^*)^T. \tag{10}$$

By using (6), (7), and (10), the Euclidean homography can be rewritten as follows:

$$H = [H_{jk}] = \begin{bmatrix} \cos(\theta) + \frac{q_x n_x^*}{d^*} & -\sin(\theta) + \frac{q_x n_y^*}{d^*} & \frac{q_x n_z^*}{d^*} \\ \sin(\theta) + \frac{q_y n_x^*}{d^*} & \cos(\theta) + \frac{q_y n_y^*}{d^*} & \frac{q_y n_z^*}{d^*} \\ 0 & 0 & 1 \end{bmatrix} \tag{11}$$

where $n^* = [n_x^* n_y^* n_z^*]^T$. By examining the terms in (11), it is clear that $H(t)$ contains signals that are not directly obtained from the vision system (e.g., $\theta(t)$, $q(t)$, and d^* are not directly available from the camera image). However, the six unknown elements of $H_{jk}(t)\ \forall j = 1, 2,\ k = 1, 2, 3$ can be determined indirectly from the image coordinates by solving a set of linear equations. Specifically, by using the definition given in (2), the expression given in (9) can be rewritten as follows:

$$m_i = \underbrace{\left(\frac{x_i^*}{x_i}\right)}_{\gamma_i} H m_i^* \tag{12}$$

where $\gamma_i(t) \in \mathbb{R}$ denotes a depth ratio. By expanding (12), the following expressions can be obtained:

$$1 = \gamma_i \left(H_{11} + H_{12} m_{iy}^* + H_{13} m_{iz}^*\right) \tag{13}$$

$$m_{iy} = \gamma_i \left(H_{21} + H_{22} m_{iy}^* + H_{23} m_{iz}^*\right) \tag{14}$$

$$m_{iz} = \gamma_i m_{iz}^*. \tag{15}$$

Given that (13)–(15) will be generated for each of the three target points, a total of nine independent equations will result. Given the nine independent equations, the nine unknown parameters (i.e., $H_{jk}(t)\ \forall j = 1, 2,\ k = 1, 2, 3$ and $\gamma_i(t)\ \forall i = 1, 2, 3$) can be determined. Based on the fact that the elements of the homography matrix and the depth ratio can be determined, various techniques can now be applied [16], [37], [38] to decompose $H(t)$ to obtain $R(t)$, $\gamma_i(t)$, and $q(t)n^*/d^*$; hence, $\theta(t)$ and $\gamma_i(t)$ can be calculated and used in the subsequent control development. To compute $\theta(t)$ from $R(t)$ the following expression can be utilized [31]:

$$\theta = \cos^{-1}\left(\frac{1}{2}\left(\text{tr}(R) - 1\right)\right)$$

where

$$0 \leq \theta(t) \leq \pi.$$

Remark 1: The position and orientation of the mobile robot is not required to be known; rather, only relative translation and orientation information between two corresponding images is required to be computed as previously described in this section. The two required images consist of the current image and an *a priori* acquired image (i.e., the desired image). The requirement for an *a priori* desired image of a target is mild. For example, a mobile robot could be guided (e.g., via a teach pendent) to a desired relative position and orientation with respect to a (indoor or outdoor) target where the desired image is then taken. For future tasks, the mobile robot can compare the current image to the previously acquired image to autonomously return to the desired relative position and orientation, based on the subsequent control development.

Remark 2: In practice, caution has to be given to determine a unique solution for $\theta(t)$ from the homography decomposition. To determine the unique solution for $\theta(t)$ from the set of possible solutions generated by the homography decomposition (e.g., using the Faugeras decomposition algorithm), a best guess estimate of the constant normal n^* can be selected from the physical relationship between the camera and the plane defined by the object feature points. Of the possible solutions generated for n^* by the decomposition algorithm, the solution that yields the minimum norm difference with the initial best guess can be determined as the correct solution. The solution that most closely matches the best guess estimate can then be used to determine the correct solutions for $\theta(t)$. The robustness of the system is not affected by the *a priori* best guess estimate of n^* since the estimate is only used to resolve the ambiguity in the solutions generated by the decomposition algorithm.

IV. Problem Formulation

The control objective is to ensure that the coordinate frame attached to the mobile robot is regulated to the fixed coordinate frame $\mathcal{F}^*$. This objective is naturally defined in terms of the Euclidean position/orientation of the mobile robot. Specifically, the translation error between $\mathcal{F}$ and $\mathcal{F}^*$, denoted by $e_t(t) \in \mathbb{R}^2$, can be written for any target point O_i, $i = 1, 2, 3$ as follows:

$$e_t \triangleq \begin{bmatrix} e_{tx} \\ e_{ty} \end{bmatrix} = \begin{bmatrix} q_x \\ q_y \end{bmatrix} = \begin{bmatrix} x_i \\ y_i \end{bmatrix} - \begin{bmatrix} \cos(\theta) & -\sin(\theta) \\ \sin(\theta) & \cos(\theta) \end{bmatrix} \begin{bmatrix} x_i^* \\ y_i^* \end{bmatrix} \tag{16}$$

where (5)–(7) have been utilized. The orientation error between $\mathcal{F}$ and $\mathcal{F}^*$, denoted by $e_o(t) \in \mathbb{R}$, can be written as follows:

$$e_o(t) \triangleq \theta(t) \tag{17}$$

where θ was defined in (6). Based on the definitions of (16) and (17), the control objective is to regulate $e_t(t)$ and $e_o(t)$ to zero. The open-loop error system for $e_t(t)$ and $e_o(t)$ can be determined by taking the time derivative of (16) and (17) and then utilizing the fact that the time derivative of the Euclidean position given in (1) can be determined as follows [11], [27]:

$$\dot{\bar{m}}_i = -v - \omega \times \bar{m}_i \tag{18}$$

where $v(t)$, $\omega(t) \in \mathbb{R}$ denote the linear and angular velocity of the mobile robot expressed in $\mathcal{F}$ as

$$\begin{aligned} v(t) &\triangleq [v_c(t) \quad 0 \quad 0]^T \\ \omega(t) &\triangleq [0 \quad 0 \quad \omega_c(t)]^T \\ &= \left[0 \quad 0 \quad -\dot{\theta}(t)\right]^T \end{aligned} \tag{19}$$

respectively. From the expression given in (1), (18), and (19), the Euclidean mobile robot velocity can be written in terms of the linear and angular velocity as follows:

$$\begin{aligned} \dot{x}_i &= -v_c + y_i \omega_c \\ \dot{y}_i &= -x_i \omega_c. \end{aligned} \tag{20}$$

After utilizing (16), (19), and (20) the following open-loop error system can be obtained:

$$\begin{aligned} \dot{e}_{tx} &= -v_c + \omega_c e_{ty} \\ \dot{e}_{ty} &= -\omega_c e_{tx} \\ \dot{e}_o &= -\omega_c \end{aligned} \tag{21}$$

where (16) was utilized.

V. Control Development

The structure of the resulting open-loop error system developed in (21) has been extensively examined in mobile robot control literature. However, unlike the typical mobile robot control problem,[1] the Euclidean translation error signals $e_{tx}(t)$ and $e_{ty}(t)$ are unmeasurable, and hence, new analytical development is required to overcome this conundrum. To address this issue, an adaptive controller is developed in this section that actively compensates for the unknown depth information through a gradient-based adaptive update law.

A. Control Design

To facilitate the subsequent control design,[2] a composite translation and rotation error signal, denoted by $r(t) \in \mathbb{R}^3$, is defined as follows:

$$r \triangleq [r_1(t) \quad r_2(t) \quad r_3(t)] = \left[-e_o \quad -\frac{e_{tx}}{x_i^*} \quad \frac{e_{ty}}{x_i^*}\right]. \tag{22}$$

By utilizing the relationship introduced in (16), the following expressions can be developed for $r_2(t)$ and $r_3(t)$:

$$r_2 = -\left[\frac{1}{\gamma_i} - \cos(\theta) + m_{iy}^* \sin(\theta)\right] \tag{23}$$

$$r_3 = \left[\frac{1}{\gamma_i} m_{iy} - \sin(\theta) - m_{iy}^* \cos(\theta)\right]. \tag{24}$$

From the expressions given in (22)–(24), it is clear that $r_1(t)$, $r_2(t)$, and $r_3(t)$ can be computed from (13)–(15) and the decomposition of the homography matrix. After taking the time derivative of (22) and utilizing (21), the resulting simplified open-loop dynamics for $r(t)$ can be determined as follows:

$$\begin{aligned} \dot{r}_1 &= \omega_c \\ \alpha \dot{r}_2 &= v_c - \alpha \omega_c r_3 \\ \dot{r}_3 &= \omega_c r_2 \end{aligned} \tag{25}$$

where (22) has been utilized, and $\alpha \in \mathbb{R}$ denotes the following positive constant:

$$\alpha \triangleq x_i^*. \tag{26}$$

To further facilitate the subsequent control design and analysis, an auxiliary signal $\eta(t) \in \mathbb{R}$ is designed as

$$\eta \triangleq r_2 - r_3 \sin(t) \tag{27}$$

where the following open-loop dynamics for $\eta(t)$ can be determined by using (25):

$$\alpha \dot{\eta} = v_c - \alpha r_3 \omega_c - \alpha \sin(t) \omega_c r_2 - \alpha r_3 \cos(t). \tag{28}$$

[1]See the results in [15] for an example of how a classic control strategy motivated by [28] can be proven to yield asymptotic stability using a monocular camera systems as feedback. Specifically, Lyapunov-based analysis techniques are used to prove the asymptotic result despite the fact that controller does not compensate for the effects of an unknown depth parameter.

[2]The proposed controller is inspired by the development presented in [32].

Based on the open-loop dynamics of (25) and (28), and the subsequently stability analysis, an adaptive kinematic controller can be designed as follows:

$$v_c = -k_2 \eta + \hat{\alpha} r_3 \cos(t) + \hat{\alpha} \omega_c r_3 \tag{29}$$

$$\omega_c = -k_1 (r_1 + \chi) \tag{30}$$

where $k_1, k_2 \in \mathbb{R}$ denote positive control gains, and $\chi(t) \in \mathbb{R}$ is an auxiliary signal defined as follows:

$$\chi = (\eta + r_3 \sin(t))(r_3 - \eta \sin(t)). \tag{31}$$

In (29), $\hat{\alpha}(t) \in \mathbb{R}$ denotes a dynamic estimate of α generated by the following differential expression:

$$\dot{\hat{\alpha}} = \Gamma(-r_3 \eta \cos(t) - \omega_c \eta r_3) \tag{32}$$

where $\Gamma \in \mathbb{R}$ denotes a positive adaptation gain. After substituting the control inputs given in (29) and (30) into (25) and (28), respectively, the following closed-loop error system is obtained:

$$\begin{aligned} \dot{r}_1 &= -k_1 (r_1 + \chi) \\ \alpha \dot{\eta} &= -k_2 \eta - \tilde{\alpha}(r_3 \cos(t) + w_c r_3) + \alpha k_1 r_2 \sin(t)(r_1 + \chi) \\ \dot{r}_3 &= -k_1 r_2 (r_1 + \chi) \end{aligned} \tag{33}$$

where $\tilde{\alpha}(t) \in \mathbb{R}$ denotes the following parameter estimation error:

$$\tilde{\alpha} = \alpha - \hat{\alpha}. \tag{34}$$

B. Stability Analysis

Theorem 1: The control law given in (29) and (30) ensures that the position and orientation of the mobile robot coordinate frame $\mathcal{F}$ is regulated to the desired position/orientation described by $\mathcal{F}^*$ in the sense that

$$\lim_{t \to \infty} e_t(t),\ e_o(t) = 0. \tag{35}$$

Proof: To prove (35), we define the following nonnegative function $V(t)$:

$$V \triangleq \frac{1}{2}\alpha \left(r_1^2 + \eta^2 + r_3^2\right) + \frac{1}{2}\Gamma^{-1}\tilde{\alpha}^2. \tag{36}$$

After taking the time derivative of (36) and substituting for the closed-loop system of (33), the following expression is obtained:

$$\begin{aligned} \dot{V} = &-k_1 \alpha r_1 (r_1 + \chi) - k_1 \alpha r_2 r_3 (r_1 + \chi) - \Gamma^{-1} \tilde{\alpha} \dot{\hat{\alpha}} + \eta \\ &\times [-k_2 \eta - \tilde{\alpha}(r_3 \cos(t) + \omega_c r_3) + \alpha k_1 r_2 \sin(t)(r_1 + \chi)]. \end{aligned} \tag{37}$$

After substituting (32) into (37) and cancelling common terms, we have

$$\dot{V} = -k_2 \eta^2 - \alpha k_1 (r_1 + \chi)^2 \tag{38}$$

where (27) and (31) have been utilized. From (36) and (38), $r_1(t)$, $r_3(t)$, $\eta(t)$, $\tilde{\alpha}(t) \in \mathcal{L}_\infty$ and $\eta(t)$, $[r_1(t) + \chi(t)] \in \mathcal{L}_2$. Based on the previous facts, (27)–(31), (33), and (34) can be used to determine that $\chi(t)$, $\hat{\alpha}(t)$, $\omega_c(t)$, $v_c(t)$, $r_2(t)$, $\dot{r}_1(t)$,

$\dot{r}_3(t), \dot{\eta}(t) \in \mathcal{L}_\infty$. Based on the facts that $r_1(t), r_2(t), r_3(t) \in \mathcal{L}_\infty$ and that x_i^* is a positive constant, (22) can be used to prove that $e_o(t), e_{tx}(t), e_{ty}(t) \in \mathcal{L}_\infty$. The expressions in (32) and (34) can be used to prove that $\dot{\tilde{\alpha}}(t), \dot{\hat{\alpha}}(t) \in \mathcal{L}_\infty$. Since $\dot{r}_3(t)$ and $\dot{\tilde{\alpha}}(t) \in \mathcal{L}_\infty$, then $r_3(t)$, $\tilde{\alpha}(t)$ are uniformly continuous (UC). After taking the time derivative of (31), the following expression can be obtained:

$$\dot{\chi} = (\dot{\eta} + \dot{r}_3 \sin(t) + r_3 \cos(t))(r_3 - \eta \sin(t)) + (\eta + r_3 \sin(t))(\dot{r}_3 - \dot{\eta} \sin(t) - \eta \cos(t)). \quad (39)$$

From the previous facts and (39), $\dot{\chi}(t) \in \mathcal{L}_\infty$. Based on the facts that $\eta(t), \dot{\eta}(t), [r_1(t)+\chi(t)], [\dot{r}_1(t)+\dot{\chi}(t)] \in \mathcal{L}_\infty$ and that $\eta(t)$, $[r_1(t)+\chi(t)] \in \mathcal{L}_2$, Barbalat's lemma [29] can be employed to conclude that

$$\lim_{t\to\infty} \eta(t), [r_1(t) + \chi(t)] = 0. \quad (40)$$

The result in (40) can be used in conjunction with the closed-loop dynamics for $r_1(t)$ and $r_3(t)$ given in (33) and the control input of (30), to determine that

$$\lim_{t\to\infty} \dot{r}_1(t), \omega_c(t), \dot{r}_3(t) = 0. \quad (41)$$

By utilizing (30), the second equation of (33) can be rewritten as follows:

$$\alpha \dot{\eta} = [-k_2 \eta - \tilde{\alpha} \omega_c r_3 - \alpha r_2 \sin(t) \omega_c] - \tilde{\alpha} r_3 \cos(t). \quad (42)$$

The results in (40) and (41) can be used to determine that the bracketed term of (42) goes to zero as $t \to \infty$; therefore, since $\tilde{\alpha}(t)$, $r_3(t)$ are UC and $\eta(t)$ has a finite limit as $t \to \infty$, the extended Barbalat's lemma (see the Appendix) can be invoked to prove that

$$\lim_{t\to\infty} \dot{\eta}(t) = 0. \quad (43)$$

After taking the time derivative of $[r_1(t) + \chi(t)]$, substituting (33) and (39) for $\dot{r}_1(t)$ and $\dot{\chi}(t)$, respectively, the following resulting expression can be obtained:

$$\frac{d}{dt}[r_1(t) + \chi(t)] = [-k_1(r_1 + \chi) + \vartheta(t)] + r_3^2 \cos(t) \quad (44)$$

where the auxiliary signal $\vartheta(t) \in \mathbb{R}$ is defined as follows:

$$\vartheta(t) \triangleq (\eta + r_3 \sin(t))(\dot{r}_3 - \dot{\eta} \sin(t) - \eta \cos(t)) + r_3(\dot{\eta} + \dot{r}_3 \sin(t)) - \eta \sin(t)(\dot{\eta} + \dot{r}_3 \sin(t) + r_3 \cos(t)). \quad (45)$$

Based on (40), (41), and (43), we have

$$\lim_{t\to\infty} \vartheta(t) = 0. \quad (46)$$

From (40) and (46), the bracketed term of (44) also goes to zero as $t \to \infty$. Since $r_3(t)$ is UC and $[r_1(t)+\chi(t)]$ has a finite limit as $t \to \infty$, the extended Barbalat's lemma (see the Appendix) can be utilized to conclude that

$$\lim_{t\to\infty} r_3^2 \cos(t) = 0. \quad (47)$$

Fig. 3. Mobile robot testbed.

The result in (47) implies that

$$\lim_{t\to\infty} r_3(t) = 0. \quad (48)$$

Based on the previous facts, (31) and (40) can now be

$$\lim_{t\to\infty} r_1(t) = 0. \quad (49)$$

By utilizing (40), (48), (49), and the definitions introduced in (22) and (27), the result in (35) can be obtained. Specifically, given that

$$\lim_{t\to\infty} r_1(t), r_3(t), \eta(t) = 0$$

then it can be determined that

$$\lim_{t\to\infty} e_t(t), e_o(t) = 0.$$

VI. Experimental Verification

A. Testbed

The testbed depicted in Fig. 3 was constructed to implement the adaptive regulation controller given by (29), (30), and (32). The mobile robot testbed consists of the following components: a modified K2A mobile robot [with an inclusive Pentium 133-MHz personal computer (PC)] manufactured by Cybermotion Inc., a Dalsa CAD-6 camera that captures 955 frames per second with eight-bit grayscale at a 260 × 260 resolution, a Road Runner Model 24 video capture board, and two Pentium-based PCs. In addition to the mobile robot modifications described in detail in [14], additional modifications particular to this experiment included mounting a camera and the associated image processing Pentium IV 800-MHz PC (operating under QNX, a real-time micro-kernel based operating system) on the top of the mobile robot as depicted in Fig. 3. The internal mobile robot computer (also operating under QNX) hosts the control algorithm that was written in C/C++ and implemented using Qmotor 3.0 [23]. In addition to the image processing PC, a second PC (operating under the MS Windows 2000 operating system) was used to remotely

login to the internal mobile robot PC via the QNX Phindows application. The remote PC was used to access the graphical user interface of Qmotor for execution of the control program, gain adjustment, and data management, plotting, and storage. Light-emitting diodes (LEDs) were rigidly attached to a rigid structure that was used as the target, where the intensity of the LEDs contrasted sharply with the background. Due to the contrast in intensity, a simple thresholding algorithm was used to determine the coordinates of each LED.

The mobile robot is controlled by a torque input applied to the drive and steer motors. As subsequently described, to facilitate a torque controller the actual linear and angular velocity of the mobile robot is required. To acquire these signals a backward difference algorithm was applied to the drive and steering motor encoders. Encoder data acquisition and the control implementation were performed at a frequency of 1.0 kHz using the Quanser MultiQ I/O board. For simplicity the electrical and mechanical dynamics of the system were not incorporated in the control design (i.e., the emphasis of this experiment is to illustrate the visual servo controller). However, since the developed kinematic controller is differentiable, standard backstepping techniques could be used to incorporate the mechanical and electrical dynamics. See [13] and [14] for several examples that incorporate the mechanical dynamics. Permanent magnet dc motors provide steering and drive actuation through a $106:1$ and a $96:1$ gear coupling, respectively. The modified K2A mobile robot has an approximate mass of 165 [kg], an inertia of approximately 4.643 $[\text{kg}\cdot\text{m}^2]$, and a wheel radius of $r_o = 0.010$ [m]. Using the Camera Calibration Toolbox for Matlab (Zhengyou Zhang's data) [2] the intrinsic calibration parameters of the camera were determined. The pixel coordinates of the principal point (i.e., the image center that is defined as the frame buffer coordinates of the intersection of the optical axis with the image plane) were determined to be $u_0 = v_0 = 130$ [pixels], the focal length and camera scaling factors were determined to be $fk_u = 1229.72$ [pixels] and $fk_v = 1235.29$ [pixels].

B. Results

Based on (22)–(24), (27), (29), (30), and (32) the signals required to implement the controller include m_{1y}^*, $\gamma_1(t)$, $\theta(t)$, and $m_{1y}(t)$.[3] As previously described, to obtain these signals an image is required to be obtained at the desired relative position and orientation of the camera with respect to a target. The mobile robot was driven by a joystick to a desired position and orientation relative to the target, the desired image was acquired, and the coordinates of the target features were saved on the image processing PC. From the coordinates of the target features and knowledge of the intrinsic calibration parameters, (4) was used to determine m_{1y}^*. The constant value for m_{1y}^* was included in the control code hosted by the internal mobile robot PC. After obtaining the desired image, the mobile robot was driven away from the target by joystick approximately 6 [m] along the x axis, with some small offset along the y axis, and with approximately 34 [deg] of orientation error. Before the control program was executed, the image processing PC was set to acquire the live camera images at 955 frames/s,[4] to determine the pixel coordinates of the target points, to construct and decompose the homography, and to transmit the signals $\gamma_1(t)$, $\theta(t)$, and $m_{1y}(t)$ that are computed from the homography decomposition via a server program over a dedicated 100 Mb/s network connection to the internal mobile robot computer. A client program was executed on the internal mobile robot computer to receive $\gamma_1(t)$, $\theta(t)$, and $m_{1y}(t)$ from the server program and write the information into a shared memory location. When the control program was executed, the values for $\gamma_1(t)$, $\theta(t)$, and $m_{1y}(t)$ were acquired from the shared memory location (rather than directly from the network connection to maintain a near deterministic response and for program stability). The values for m_{1y}^*, $\gamma_1(t)$, $\theta(t)$, and $m_{1y}(t)$ were utilized to determine $r(t)$ and $\eta(t)$ as described by (22)–(24) and (27), and to compute the control signals.

To execute a torque level controller, a feedback loop was implemented as follows:

$$\tau = K_h \bar{\eta} \tag{50}$$

where $\tau = [\tau_1(t), \tau_2(t)]^T \in \mathbb{R}^2$ denotes a vector of the drive and steering motor torques, respectively, $K_h \in \mathbb{R}^{2\times 2}$ is a diagonal scaling term, and $\bar{\eta}(t) \in \mathbb{R}^2$ is a velocity mismatch signal defined as

$$\bar{\eta} = [v_c \quad \omega_c]^T - [v_a \quad \omega_a]^T \tag{51}$$

where $v_c(t)$ and $\omega_c(t)$ denote the linear and angular velocity inputs computed in (29) and (30), and $v_a(t)$ and $\omega_a(t)$ denote actual linear and angular velocity of the mobile robot computed from the time derivative of the motor encoders.

The control and adaptation gains were adjusted to reduce the position/orientation error with the initial adaptive estimate set to zero.[5] The final feedback and adaptation gain values were recorded as follows:

$$k_1 = 55.35 \quad k_2 = 21.25 \quad \Gamma = 0.15 \quad K_h = diag\{8, 0.185\}. \tag{52}$$

The resulting orientation error is provided in Fig. 4, and the unitless planar position regulation errors $r_2(t)$ and $r_3(t)$, are depicted in Fig. 5. Fig. 6 illustrates that the adaptive estimate for the depth parameter d^* approaches a constant. From Figs. 4 and 5, it is clear that some steady state errors exist in the orientation and the translation along the lateral mobile robot axis, previously defined as $e_o(t)$ and $e_{ty}(t)$, respectively. The steady-state error in $e_o(t)$ is due, in large part, to the fact that as the mobile robot approaches the target, changes in the image-space orientation are magnified (i.e., a one-pixel difference from a far distance has less orientation error than a one-pixel difference at a close distance). The steady-state error in $e_o(t)$ is propagated in

[3]The subscript $i = 1$, is used to indicate that the signal corresponds to the first target point (without loss of generality).

[4]A camera with an image capture rate of 955 frames/s is not required for the experiment. The high-speed camera was utilized to enable a higher closed-loop control frequency.

[5]In practice, the adaptive estimate would be initialized to a best guess value. In this experiment, the adaptive estimate was initialized to zero to illustrate the ability of the estimate to converge in the presence of a large initial error.

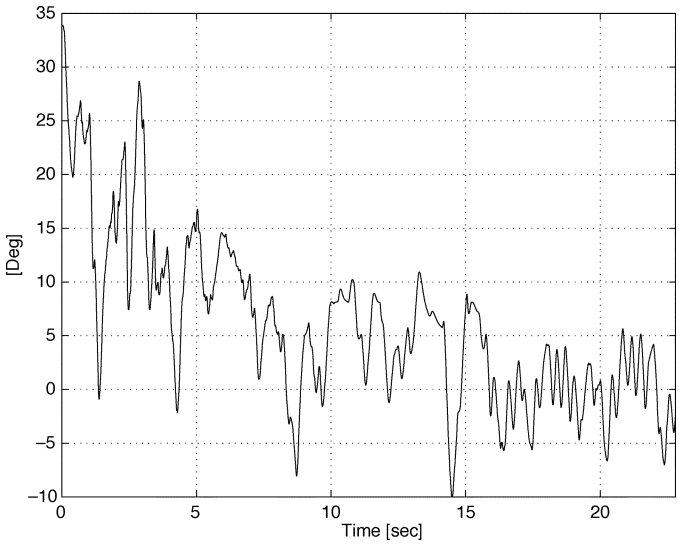

Fig. 4. Orientation error, $e_o(t) = r_1(t)$.

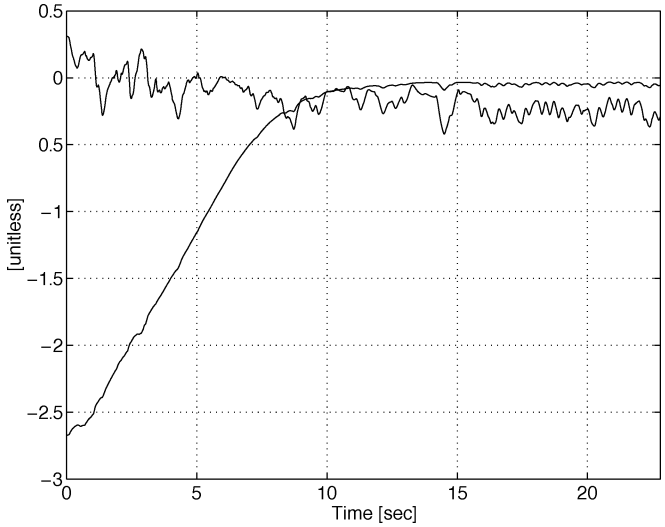

Fig. 5. Position error, $r_2(t)$ and $r_3(t)$.

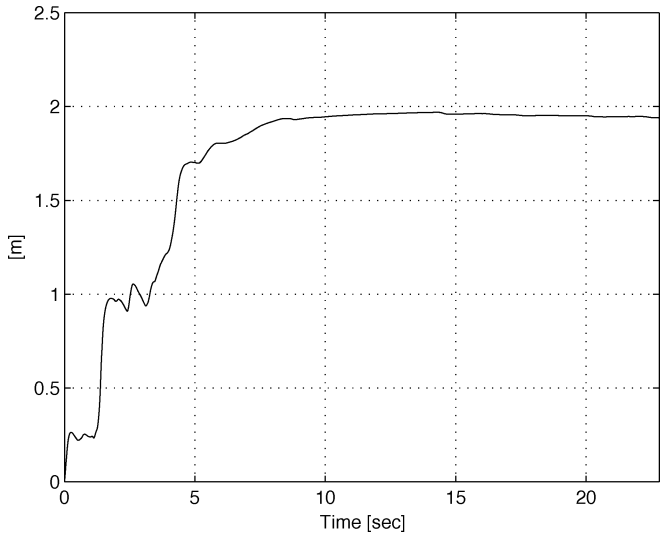

Fig. 6. Adaptive estimate.

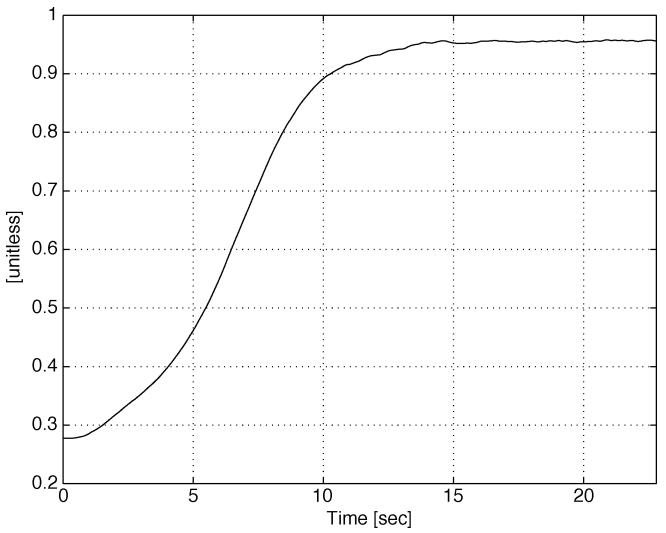

Fig. 7. Computed depth ratio.

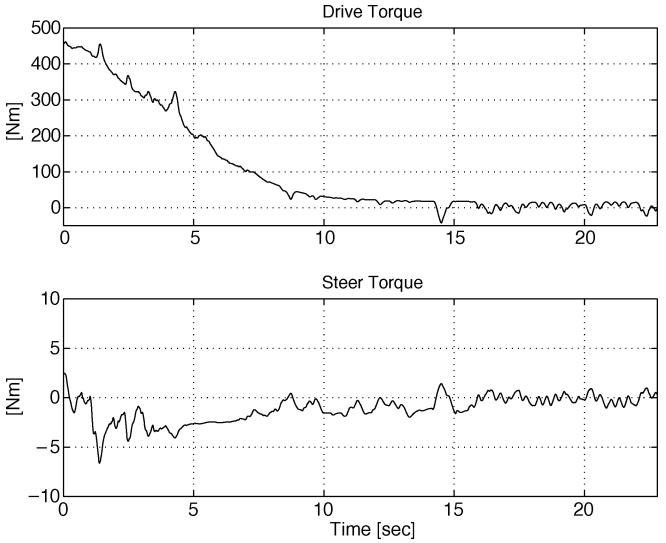

Fig. 8. Computed torque inputs.

$e_{ty}(t)$. That is, the lateral position of the mobile robot is directly influenced by the orientation error. The computed unitless depth ratio $\gamma_1(t)$ is provided in Fig. 7. The control torque inputs at the wheels of the mobile robot (i.e., after the $106:1$ and $96:1$ gear coupling) that is applied by the steer and drive motors is depicted in Fig. 8.

VII. Conclusion

In this paper, asymptotic regulation of the position/orientation of a mobile robot is achieved with a monocular vision system. By comparing the features of an object from an initial snapshot to features of the object in the current image, geometric relationships are exploited to determine a Euclidean homography. The Euclidean homography relates the image-space feedback to the actual Euclidean position/orientation of the camera (and hence the mobile robot) in a local coordinate system. By decomposing the homography into separate translation and rotation components, we were able to exploit reconstructed 3-D task-space information to construct a kinematic controller. The performance

of the developed controller was demonstrated through experimental results. The impact of these results are that a new analytical approach has been developed using homography-based concepts to enable a mobile robot to be regulated to a desired position/orientation based on a desired image, despite the lack of depth measurements. A practical issue with the presented research is that the feature points may leave the camera's field of view during task execution. To address this problem, future efforts will target regulating the mobile robot while ensuring the feature points remain visible. Our future efforts will also target the development of Lyapunov-based analytical methods that enable adaptive/robust techniques to be employed to compensate for the uncertainty associated with the camera calibration parameters.

APPENDIX

The extended Barbalat's lemma was utilized in the stability analysis for Theorem 1. This lemma is stated as follows, and a proof for the lemma can be found in [14].

Lemma 2: If a differentiable function $f(t) \in \mathbb{R}$ has a finite limit as $t \to \infty$, and its time derivative can be written as follows:

$$\dot{f}(t) = g_1(t) + g_2(t) \tag{53}$$

where $g_1(t)$ is a uniformly continuous function and

$$\lim_{t\to\infty} g_2(t) = 0 \tag{54}$$

then

$$\lim_{t\to\infty} \dot{f}(t) = 0 \quad \lim_{t\to\infty} g_1(t) = 0. \tag{55}$$

REFERENCES

[1] S. Baker and S. Nayar, "A theory of catadioptric image formation," in *Proc. ICCV*, Jan. 1998, pp. 35–42.

[2] J.-Y. Bouguet, Camera Calibration Toolbox for Matlab. Public Domain Internet Software.

[3] D. Burschka and G. Hager, "Vision-based control of mobile robots," in *Proc. IEEE Int. Conf. Robotics and Automation*, 2001, pp. 1707–1713.

[4] F. Chaumette and E. Malis, "2 1/2 D visual servoing: A possible solution to improve image-based and position-based visual servoings," in *Proc. IEEE Int. Conf. Robotics and Automation*, 2000, pp. 630–635.

[5] F. Chaumette, E. Malis, and S. Boudet, "2D 1/2 visual servoing with respect to a planar object," in *Proc. Workshop on New Trends in Image-Based Robot Servoing*, 1997, pp. 45–52.

[6] J. Chen, W. E. Dixon, D. M. Dawson, and M. McIntyre, "Homography-based visual servo tracking control of a wheeled mobile robot," *IEEE Trans. Robot.*, to be published.

[7] J. Chen, D. M. Dawson, W. E. Dixon, and A. Behal, "Adaptive homography-based visual servo tracking for fixed and camera-in-hand configurations," *IEEE Trans. Contr. Syst. Technol.*, to be published.

[8] F. Conticelli and B. Allotta, "Nonlinear controllability and stability analysis of adaptive image-based systems," *IEEE Trans. Robot. Autom.*, vol. 17, no. 2, pp. 208–214, Apr. 2001.

[9] P. I. Corke and S. A. Hutchinson, "A new hybrid image-based visual servo control scheme," in *Proc. IEEE Conf. Decision and Control*, 2000, pp. 2521–2527.

[10] A. K. Das *et al.*, "Real-time vision-based control of a nonholonomic mobile robot," in *Proc. IEEE Int. Conf. Robotics and Automation*, 2001, pp. 1714–1719.

[11] K. Deguchi, "Optimal motion control for image-based servoing by decoupling translation and rotation," in *Proc. Int. Conf. Intelligent Robots and Systems*, Oct. 1998, pp. 705–711.

[12] W. E. Dixon, D. M. Dawson, E. Zergeroglu, and A. Behal, "Adaptive tracking control of a wheeled mobile robot via an uncalibrated camera system," in *Proc. IEEE American Control Conf.*, Chicago, IL, Jun. 2000, pp. 1493–1497.

[13] W. E. Dixon, M. S. de Queiroz, D. M. Dawson, and T. J. Flynn, "Adaptive tracking and regulation control of a wheeled mobile robot with controller/update law modularity," *IEEE Trans. Contr. Syst. Technol.*, vol. 12, no. 1, pp. 138–147, Jan. 2004.

[14] W. E. Dixon, D. M. Dawson, E. Zergeroglu, and A. Behal, *Nonlinear Control of Wheeled Mobile Robots*. Berlin, Germany: Springer-Verlag, 2001.

[15] Y. Fang, D. M. Dawson, W. E. Dixon, and M. S. de Queiroz, "2.5D visual servoing of wheeled mobile robots," in *Proc. IEEE Conf. Decision and Control*, Dec. 2002, pp. 2866–2871.

[16] O. Faugeras and F. Lustman, "Motion and structure from motion in a piecewise planar environment," *Int. J. Pattern Recognit. Artif. Intell.*, vol. 2, no. 3, pp. 485–508, 1988.

[17] G. D. Hagar, D. J. Kriegman, A. S. Georghiades, and O. Ben-Shahar, "Toward domain-independent navigation: Dynamic vision and control," in *Proc. IEEE Conf. Decision and Control*, 1998, pp. 3257–3262.

[18] M. Hebert, "3-D vision for outdoor navigation by an autonomous vehicle," presented at the *Image Understanding Workshop*, Cambridge, U.K., 1998.

[19] D. Jung, J. Heinzmann, and A. Zelinsky, "Range and pose estimation for visual servoing of a mobile robot," in *Proc. IEEE Int. Conf. Robotics and Automation*, 1998, pp. 1226–1231.

[20] B. H. Kim *et al.*, "Localization of a mobile robot using images of a moving target," in *Proc. IEEE Int. Conf. Robotics Automation*, 2001, pp. 253–258.

[21] D. J. Kriegman, E. Triendl, and T. O. Binford, "Stereo vision navigation in buildings for mobile robots," *IEEE Trans. Robot. Autom.*, vol. 5, no. 6, pp. 792–803, Dec. 1989.

[22] Y. Ma, J. Kosecka, and S. Sastry, "Vision guided navigation for nonholonomic mobile robot," *IEEE Trans. Robot. Autom.*, vol. 15, no. 3, pp. 521–536, Jun. 1999.

[23] M. S. Loffler, N. P. Costescu, and D. M. Dawson, "Qmotor 3.0 and the Qmotor robotic toolkit: a PC-based control platform," *IEEE Contr. Syst. Mag.*, vol. 22, no. 3, pp. 12–26, Jun. 2002.

[24] R. Mahony and T. Hamel, "Visual servoing using linear features for under-actuated rigid body dynamics," in *Proc. IEEE/RJS Int. Conf. Intelligent Robots and Systems*, 2001, pp. 1153–1158.

[25] E. Malis, "Contributions à la modélization et à la commande en asservissement visuel," Ph.D. dissertation, Univ. Rennes I, IRISA, Paris, France, Nov. 1998.

[26] E. Malis and F. Chaumette, "2 1/2 D visual servoing with respect to unknown objects through a new estimation scheme of camera displacement," *Int. J. Comput. Vis.*, vol. 37, no. 1, pp. 79–97, Jun. 2000.

[27] E. Malis, F. Chaumette, and S. Bodet, "2 1/2 D visual servoing," *IEEE Trans. Robot. Autom.*, vol. 15, no. 2, pp. 238–250, Apr. 1999.

[28] C. Samson, "Velocity and torque feedback control of a nonholonomic cart," presented at the *Int. Workshop in Adaptive and Nonlinear Control: Issues in Robotics*, Grenoble, France, 1990.

[29] J. J. Slotine and W. Li, *Applied Nonlinear Control*. Englewood Cliffs, NJ: Prentice-Hall, 1991.

[30] K.-T. Song and J.-H. Huang, "Fast optical flow estimation and its application to real-time obstacle avoidance," in *Proc. IEEE Int. Conf. Robotics and Automation*, 2001, pp. 2891–2896.

[31] M. W. Spong and M. Vidyasagar, *Robot Dynamic and Control*. New York: Wiley, 1989.

[32] A. R. Teel, R. M. Murray, and C. G. Walsh, "Non-holonomic control systems: From steering to stabilization with sinusoids," *Int. J. Contr.*, vol. 62, no. 4, pp. 849–870, 1995.

[33] C. E. Thorpe, M. Hebert, T. Kanade, and S. Shafer, "Vision and navigation for the Carnegie-Mellon Navlab," *IEEE Trans. Pattern Anal. Mach. Intell.*, vol. 10, no. 3, pp. 362–373, May 1988.

[34] M. A. Turk, D. G. Morgenthaler, K. D. Gremban, and M. Marra, "VITS-A vision system for autonomous land vehicle navigation," *IEEE Trans. Pattern Anal. Mach. Intell.*, vol. 10, no. 3, pp. 342–361, May 1988.

[35] H. Y. Wang, S. Itani, T. Fukao, and N. Adachi, "Image-based visual adaptive tracking control of nonholonomic mobile robots," in *Proc. IEEE/RJS Int. Conf. Intelligent Robots and Systems*, 2001, pp. 1–6.

[36] A. M. Waxman *et al.*, "A visual navigation system for autonomous land vehicles," *IEEE J. Robot. Autom.*, vol. RA-3, no. 2, pp. 124–141, Apr. 1987.

[37] Z. Zhang and A. R. Hanson, "Scaled Euclidean 3D reconstruction based on externally uncalibrated cameras," in *IEEE Symp. Computer Vision*, 1995.

[38] H. Zhang and J. P. Ostrowski, "Visual servoing with dynamics: Control of an unmanned blimp," in *Proc. IEEE Int. Conf. Robotics and Automation*, 1999, pp. 618–623.

Yongchun Fang (S'00–M'02) received the B.S degree in electrical engineering and the M.S. degree in control theory and applications from Zhejiang University, Zhejiang, China, in 1996 and 1999, respectively, and the Ph.D. degree in electrical engineering from Clemson University, Clemson, SC, in 2002.

From 2002 to 2003, he was a Postdoctoral Fellow at the Mechanical and Aerospace Engineering Department, Cornell University. He joined the Institute of Robotics and Automatic Information System, Nankai University, Tianjin, China, in 2003, where has been a Professor since then. His research interests include nonlinear control, visual servoing, and control of underactuated systems including overhead cranes.

Warren E. Dixon (S'94–M'00) received the Ph.D. degree from Clemson University. Clemson, SC, in 2000.

After completing his doctoral studies, he was selected as a Eugene P. Wigner Fellow at Oak Ridge National Laboratory where he worked in the Robotics and Energetic Systems Group of the Engineering Science and Technology Division. In 2004, he joined the faculty of the Mechanical and Aerospace Engineering Department, University of Florida. His main research interest has been the development and application of Lyapunov-based control techniques for mechatronic systems, resulting in several books and approximately 100 refereed journal and conference papers. Recent publications have focused on Lyapunov-based control of nonlinear systems including visual servoing systems, robotic systems, underactuated systems, and nonholonomic systems.

Dr. Dixon is currently an Associate Editor for IEEE TRANSACTIONS ON SYSTEMS, MAN, AND CYBERNETICS: PART B—CYBERNETICS.

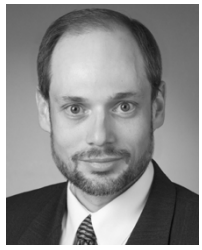

Darren M. Dawson (S'89–M'90–SM'94) received the B.S. and Ph.D. degrees in electrical engineering from the Georgia Institute of Technology (Georgia Tech), Atlanta, in 1984 and 1990, respectively.

He then worked for Westinghouse as a Control Engineer from 1985 to 1987. In July 1990, he joined the Electrical and Computer Engineering Department, Georgia Tech, where he currently holds the position of McQueen Quattlebaum Professor. His research interests include nonlinear control techniques for mechatronic applications such as electric machinery, robotic systems, aerospace systems, acoustic noise, underactuated systems, magnetic bearings, mechanical friction, paper handling/textile machines, flexible beams/robots/rotors, cable structures, and vision-based sytems. He also focuses on the development of real-time hardware and software systems for control implementation.

Prakash Chawda (S'03) received the M.S. degree from Clemson University, Clemson, SC, in 2004.

In 2003, he was selected for the reputed HERE Program as an intern at Oak Ridge National Laboratory, where he worked in the Robotics and Energetic Systems Group of the Engineering Science and Technology Division. His research work was directed at the development and application of Lyapunov-based visual servo control techniques of mechatronic systems.